Triple-Pulse Voltammetry and Polarography

Carmen Serna and Angela Molina*

Departamento de Química Física, Facultad de Ciencias Químicas y Matemáticas, Universidad de Murcia, Campus de Espinardo, E-30100 Murcia, Spain

Luis Camacho* and Juan José Ruiz

Departamento de Química Física y Termodinámica Aplicada, Facultad de Ciencias, Universidad de Córdoba, c) San Alberto Magno s/n, E-14004 Córdoba, Spain

The faradaic response of a slow electron transfer to a triple pulse of potentials was derived for the planar approximations of a static mercury drop electrode and the dropping mercury electrode. The analytical solution obtained for a static mercury drop electrode is subject to no constraints in the time interval over which the different potentials are applied. The effects of the formation of the double layer have not been taken into account in the mathematical treatment. The solution obtained was verified by comparising of the analytical solution to experimentally measured *i–t* curves for some completely reversible, completely irreversible, and quasi-reversible processes, namely the reduction of Cd(II), Cr(III), and Zn(II), respectively. The use of a triple pulse of potentials to develop new voltametric and polarographic techniques, improving on the performance of double-pulse techniques, is discussed. Among these we propose the double differential pulse (DDP) technique which involves using the current function $I_1 - 2I_2 + I_3$ where I_j is the current corresponding to potential pulse E_j. We also propose the square well pulse (SWP) technique which relies on the current function $I_3 + I_2 - 2I_1$ for a time ratio $t_2/t_3 = 0.283$. Finally, the solution for the previously reported reverse differential normal pulse (RDNP) technique was obtained. The features and performance of these techniques are discussed.

INTRODUCTION

Since Barker[1] reported the earliest electrochemical techniques based on the use of pulse of potentials, their applications and variants have grown dramatically.

According to the nomenclature proposed by Osteryoung and Schreiner,[2] the techniques using a single pulse are called normal pulse (NP) voltammetry (with a static mercury drop, SDME, or solid electrode) and normal pulse (NP) polarography (using a dropping mercury electrode, DME).

Double-pulse techniques[2] combine the faradaic currents at two different potentials applied to the same drop and include reverse pulse (RP), differential pulse (DP), differential normal pulse (DNP), and DNP in the alternating pulse mode.[3-12] These techniques offer some advantages over both linear sweep potentiostatic techniques and single-pulse techniques. In fact, they provide increased signal sensitivity, with its resulting analytical advantages, and eliminate most of the charging current. Also, despite the complexity of the mathematical solutions involved, one can establish analytical criteria that allow calculation of kinetic parameters for the process.

Multistep techniques exploit the above-mentioned advantages. The most frequently used in this respect are square-wave voltammetry,[13] (which uses short-time pulses and alternating potentials), and staircase voltammetry[14-16] (which also uses short-time pulses but the potential variation is of the staircase type). However, the complexity of the diffusional problem in these techniques compels the use of numerical methods to obtaining the solutions.[13]

In this work we analyzed the faradaic response of a slow electron transfer to a triple pulse for the planar approximation to the behavior of an SMDE (voltammetry) and a DME (polarography). The analytical solution obtained for a SMDE is subject to no constraints in the time interval over which the different potentials are applied. The effects of the formation of the double layer have not been taken into account in the mathematical treatment.

In order to obtain the solutions corresponding to the third pulse of potentials we used the solution corresponding to the second pulse previously derived by Gálvez et al.[10-12] Thus, the solutions obtained for these authors were the starting point for the present work.

The validity of the solution obtained was verified by comparison of the analytical solution to experimentally measured *i–t* curves for some completely reversible, completely irreversible, and quasi-reversible processes, namely the reduction of Cd(II), Cr(III), and Zn(II), respectively.

By using a triple pulse of potentials one can develop new techniques to improve on the above-mentioned double-pulse techniques. This possibility led us to define the double differential pulse technique (DDP).

Both the DDP technique and others that can potentially be developed in this way are based on the use of a linear combination of the currents obtained at the end of each pulse of potential used. Thus, in this work we use a pulse sequence that allows one to mask a given process under given circumstances.

One other option that is analyzed in this work is a modification of the RP technique called reverse differential normal pulse (RDNP), which was previously proposed by

(1) Barker, G. C. *Fresenius' Z. Anal. Chem.* **1960**, *173*, 70.
(2) Osteryoung, J.; Schreiner, M. M. *CRC Crit. Rev. Anal. Chem.* **1988**, *19*, S1.
(3) Osteryoung, J.; Kirowa-Eisner, E. *Anal. Chem.* **1980**, *52*, 62.
(4) Aoki, K.; Osteryoung, J.; Osteryoung, R. A. *J. Electroanal. Chem. Interfacial Electrochem.* **1980**, *110*, 1.
(5) Matsuda, H. *Bull. Chem. Soc. Jpn.* **1980**, *53*, 3439.
(6) Brumleve, T. R.; O'Dea, J. J.; Osteryoung, R. A.; Osteryoung, J. *Anal. Chem.* **1981**, *53*, 702.
(7) Brumleve, T. R.; Osteryoung, J. *Anal. Chem.* **1981**, *53*, 988.
(8) Birke, R. L.; Kim, M. H.; Strassfeld, M. *Anal. Chem.* **1981**, *53*, 852.
(9) Lovric, M.; O'Dea, J. J.; Osteryoung, J. *Anal. Chem.* **1983**, *55*, 704.
(10) Gálvez, J. *Anal. Chem.* **1985**, *57*, 585.
(11) Gálvez, J.; Zapata, J.; Serna, C. *J. Electroanal. Chem. Interfacial Electrochem.* **1986**, *205*, 21.
(12) Galvez, J.; Serna, C.; Molina, A.; Camacho, L.; Ruiz, J. J. Unpublished results.
(13) O'Dea, J. J.; Osteryoung, J.; Osteryoung, R. A. *J. Phys. Chem.* **1983**, *87*, 3911.
(14) Cristie, J. H.; Lingane, P. J. *J. Electroanal. Chem.* **1965**, *10*, 176.
(15) Zipper, J. J.; Perone, S. P. *Anal. Chem.* **1973**, *45*, 452.
(16) Stefani, S.; Seeber, R. *Anal. Chem.* **1982**, *54*, 2524.

0003-2700/93/0365-0215$04.00/0

Brumleve et al.[17] As these authors acknowledge, the theoretical treatment of this technique involves determining faradaic response to a triple pulse of potential, which has not been reported to date.

The examples studied in this work are by no means all available options in developing triple-pulse techniques, which, to our minds, could be quite numerous.

EXPERIMENTAL SECTION

Potential pulses were manually generated, and i–t curves were recorded on a PAR 273 potentiostat/galvanostat attached to a 303A PARC polarographic stand. A Prowler 105 digital-memory oscilloscope was used for data acquisition. Measurements were made by using a thermostated PAR cell, the temperature of which was kept constant at 25 ± 0.1 °C.

An SMDE with an area of 0.0258 cm^2 was employed as working electrode. A saturated calomel electrode and a platinum electrode were used as reference and auxiliary electrodes, respectively.

All reagents were Merck a.g. and were used without further purification. Mercury was purified with dilute nitric acid and distilled three times in vacuum. Nitrogen gas was used for deaeration.

We complied with standard safety rules in preparing and handling all solutions and chemicals used, particularly Cd(II) and mercury. Thus, pipets were filled with the aid of rubber bulbs and mercury was purified and distilled in a gas hood and kept under water throughout. Skin contact was avoided by using rubber gloves.

A potential at which no faradaic reaction takes place is applied for 2 s in order to allow the drop to grow and the SMDE to stabilize (delay time). Then, potentials E_1, E_2, and E_3 are applied over the time intervals t_1, t_2, and t_3, respectively.

The numerical fitting involved in the calculations was done by the program SigmaPlot.[18] This program uses a nonlinear least-squares regression method based on the Marquardt–Levenger algorithm.[19] The observed deviations in the current never exceeded 5%.

THEORETICAL BACKGROUND

Consider the following charge-transfer reaction

$$A + ne^- \underset{k_b}{\overset{k_f}{\rightleftarrows}} B$$

and assume that the electrode area $q(t)$ is given by the general law

$$q(t) = q_0 t^z \qquad z \geq 0 \tag{1}$$

($z = 0$) for the planar approximation of the SMDE and $z = {}^2/_3$ for a DME) and that the operator $\hat{D}_i$ is given by

$$\hat{D}_i = \frac{\partial}{\partial t} - D_i\frac{\partial^2}{\partial x^2} - \frac{zx}{t}\frac{\partial}{\partial x} \tag{2}$$

with i = A or B.

It should also be pointed out that the theoretical treatment developed here is also valid for a solid electrode provided that the boundary conditions are renewed, either by stirring or by employing a sufficiently long delay time t_1 at an initial potential E_1 at zero faradaic current (see ref 17).

When the potential is set on a constant E_1 value from $t = 0$ (after a delay time for the SMDE) to $t = t_1$, the current–time response corresponding to the interval $0 \leq t \leq t_1$ as by Koutecky,[20,21] can be written as follows for $t = t_1$[11] (see Notation):

$$i_1(t_1) = nFq_0 t_1^z \sqrt{\frac{(2z+1)D_A}{\pi t_1}} \frac{c_A^*}{1+\gamma K_1} F_z(\chi_1) \tag{3}$$

where

$$\chi_1 = \sqrt{\frac{4t_1}{(2z+1)D_A}} k_s \frac{1+\gamma K_1}{K_1^{\alpha}} \tag{4}$$

If the potential at $t = t_1$ is stepped up to the other constant value E_2 over an interval $0 \leq \tau_2 \leq t_2$ ($t = t_1 + t_2$), the current–time response corresponding to this second pulse for $\tau_2 = t_2$ can be written[12]

$$i_2(t_1+t_2) = i_1(t_1+t_2) + nFq_o\left(\frac{D_A}{\pi t_2}\right)^{1/2}(t_1 + t_2)^z c_A^*\{Z_1 G_z(\beta_2,y_2) + \mu_2 H_z(\beta_2,y_2)\} \tag{5}$$

where

$$\mu_2 = \frac{2F_z(\chi_2)}{\sqrt{\pi}\chi_2(1+\gamma K_1)}\left(1 - \frac{1+\gamma K_1}{1+\gamma K_2}\left(\frac{K_2}{K_1}\right)^{\alpha}\right) \tag{6}$$

$$Z_1 = \frac{1}{1+\gamma K_2} - \frac{1}{1+\gamma K_1} \tag{7}$$

(see Notation for all other parameters).

We shall consider now that the potential at time $t = t_1 + t_2$ is again stepped up to the other constant value E_3 over an interval $0 \leq \tau 3 \leq t_3$. Under these conditions

$$t = t_1 + t_2 + \tau 3 \tag{8}$$

and the boundary value problem is given by

$$\hat{D}_A c_A = \hat{D}_B c_B = 0 \tag{9}$$

$$\tau 3 > 0, x \to \infty \quad \begin{cases} c_A(x,t) = c_A^* \\ c_B(x,t) = 0 \end{cases} \tag{10}$$

$$\tau 3 = 0, x \geq 0 \quad \begin{aligned} c_A(x,t) &= c_A(s1_A,\chi) + \sum_{\substack{j=0 \\ m=1}} \phi_{j,m}(s2_A)\beta^{j/2}y^m \\ c_B(x,t) &= c_B(s1_B,\chi) + \sum_{\substack{j=0 \\ m=1}} \delta_{j,m}(s2_B)\beta^{j/2}y^m \end{aligned} \tag{11}$$

where $s1_i$, $s2_i$, y, β, and χ are defined in the Notation.

$$\tau 3 > 0, x = 0 \qquad D_A\left(\frac{\partial c_A}{\partial x}\right)_{x=0} = -D_B\left(\frac{\partial c_B}{\partial x}\right)_{x=0} \tag{12}$$

$$\frac{i_3}{nFq(t)} = D_A\left(\frac{\partial c_A}{\partial x}\right)_{x=0} = \frac{k_s}{K_3^{\alpha}}(c_A(0,t) - K_3 c_B(0,t)) \tag{13}$$

where $s1_1$, $s2_1$, y, β, and χ are defined in the Notation. Equations 11 were derived in ref 12.

(17) Brumleve, T. R.; Osteryoung, R. A.; Osteryoung, J. *Anal. Chem.* **1982**, *54*, 782.
(18) *SigmaPlot*; Jandel Scientific: 65 Koch Rd., Corte Madera, CA 94925.
(19) Press, W. H.; Flannery, B. P.; Teukalsky, S. A.; Vettering, W. T. *Numerical Recipes*; University Press: Cambridge, MA 1986.
(20) Koutecky, J. *Collect. Czech. Chem. Commun.* **1953**, *18*, 597.
(21) Koutecky, J. *Czech. J. Phys.* **1953**, *2*, 50.

Equation 9 can be solved on conditions 10–13 by introducing the following variables

$$s3_1 = \frac{x}{2\sqrt{D_i \tau 3}} \tag{14}$$

$$\omega = \sqrt{\frac{4\tau 3}{D_A}} k_s \frac{1 + \gamma K_3}{K_3^{\alpha}} \tag{15}$$

$$\epsilon = \tau 3/t \qquad \lambda = \frac{\tau 3}{t_2 + \tau 3} \tag{16}$$

and adopting the following solutions for $c_A = c_B$

$$c_A(x,t) = c_A(s1_A,\chi) + \sum_{\substack{j=0 \\ m=1}} \phi_{j,m}(s2_A)\beta^{j/2}y^m + \sum_{j,k,m} \sigma_{j,k,m}(s3_A)\epsilon^{j/2}\omega^m\lambda^{k/2} \tag{17}$$

$$c_B(x,t) = c_B(s1_B,\chi) + \sum_{\substack{j=0 \\ m=1}} \delta_{j,m}(s2_B)\beta^{j/2}y^m + \sum_{j,k,m} \rho_{j,k,m}(s3_B)\epsilon^{j/2}\omega^m\lambda^{k/2} \tag{18}$$

By introducing eqs 17 and 18 in (9), we deduce, after some simplifications, the following system of recurrent differential equations:

$$\sigma''_{j,k,m}(s3_A) + 2s3_A\sigma'_{j,k,m}(s3_A) - 2(j + k + m)\sigma_{j,k,m}(s3_A) = -4zs3_A\sigma'_{j-2,k,m}(s3_A) - 2(j - 2)\sigma_{j-2,k,m}(s3_A) - 2(k - 2)\sigma_{j,k-2,m}(s3_A) \tag{19}$$

$$\rho''_{j,k,m}(s3_B) + 2s3_A\rho'_{j,k,m}(s3_B) - 2(j + k + m)\rho_{j,k,m}(s3_B) = -4zs3_B\rho'_{j-2,k,m}(s3_B) - 2(j - 2)\rho_{j-2,k,m}(s3_B) - 2(k - 2)\rho_{j,k-2,m}(s3_B) \tag{20}$$

These equations have been deduced in a general form, in such a way as they can be used for any expanding plane electrode with area given by eq 1.

The boundary conditions become

$$s3_i \to \infty \qquad \sigma_{j,k,m} = \rho_{j,k,m} = 0 \qquad \text{for } j \geq 0,\ k \geq 0,\ m \geq 0 \tag{21}$$

$$s3_i = 0 \begin{cases} \sigma'_{j,k,0} = 0 \quad \text{unless } j = 1,\ k = 0 \text{ and } j = 0,\ k = 1 & (22) \\ \sigma'_{1,0,0} = -c_A^* S \qquad \sigma'_{0,1,0} = -c_A^* D & (23) \\ \sigma'_{j,k,m} = \dfrac{\sigma_{j,k,m-1} - K_3\rho_{j,k,m-1}}{1 + \gamma K_3} \quad \text{unless } j = k = 0,\ m = 1 & (24) \\ \sigma'_{0,0,1} = c_A^* z_2 & (25) \\ \gamma\sigma'_{j,k,m} = -\rho'_{j,k,m} \quad \text{for } j \geq 0,\ k \geq 0,\ m \geq 0 & (26) \end{cases}$$

where

$$\left.\begin{aligned} S &= \frac{2}{\sqrt{\pi}}\left(1 - \frac{1 + \gamma k_3\left(\frac{k_2}{k_3}\right)^{\alpha}}{1 + \gamma k_2}\right) \times \left(\frac{Z_1 G_z(\beta,y) + \mu H_z(\beta,y)}{\sqrt{\beta}} + \frac{\sqrt{2z+1}F_z(\chi)}{1 + \gamma k_1}\right) - \frac{D}{\sqrt{\beta}} \\ D &= \frac{2}{\sqrt{\pi}}\left(1 - \frac{1 + \gamma k_3\left(\frac{k_2}{k_3}\right)^{\alpha}}{1 + \gamma k_2}\right) Z_1 G_z(\beta,y) \end{aligned}\right\} \tag{27}$$

$$\mu = \frac{2F_z(\chi)}{\sqrt{\pi}\chi(1 + \gamma k_1)}\left(1 - \frac{1 + \gamma k_1\left(\frac{k_2}{k_1}\right)^{\alpha}}{1 + \gamma k_2}\right) \tag{28}$$

$$Z_2 = \frac{1}{1 + \gamma k_3} - \frac{1}{1 + \gamma k_2} \tag{29}$$

Finally, by substituting the $\sigma_{j,k,m}(s3_A)$ functions, given in the Appendix, into eq 17 and combining it with eq 13, one obtains the current–time response corresponding to the third pulse potential, E_3:

$$i_3(t) = i_2(t) + nFq_0t^z\sqrt{\frac{D_A}{\pi t_3}}c_A^*[Z_2G_z(\epsilon,\omega) + MH_z(\epsilon,\omega) + NH_0(\lambda,\omega)] \tag{30}$$

where

$$\left.\begin{aligned} M &= \left[1 - \frac{1 + \gamma k_2\left(\frac{k_3}{k_2}\right)^{\alpha}}{1 + \gamma k_3}\right] \times \mu\left\{P_0\frac{H_z(\beta,y)}{y} - \left[1 - \frac{1 + \gamma k_2\left(\frac{k_1}{k_2}\right)^{\alpha}}{1 + \gamma k_1}\right]^{-1}\right\} \\ N &= \left[1 - \frac{1 + \gamma k_2\left(\frac{k_3}{k_2}\right)^{\alpha}}{1 + \gamma k_3}\right] Z_1 P_0 \frac{G_z(\beta,y)}{y} \end{aligned}\right\} \tag{31}$$

I–T CURVES FOR A TRIPLE PULSE

In order to check the solutions obtained we compared them to experimentally measured *i–t* curves for a triple potential pulse sequence, for three typical examples: reversible, quasi-reversible, and completely irreversible processes on an SMDE. No background (charging) currents of the supporting electrolyte were subtracted.

First, we studied the reduction of Cd(II) in 0.1 M H_2SO_4. Under these conditions, the process is reversible (E° = –610 mV)[22] and the effects of the formation of the amalgam can be considered to be negligible (these conditions are given in ref 10). In this medium, the diffusion coefficient of Cd in mercury is $D_B = 1.4 \times 10^{-5}$ cm^2 s^{-1}.[23]

Figure 1 shows the *i–t* curve for an SMDE with the following pulse sequence: First, we selected an E_1 value corresponding to the diffusion plateau of the process, i.e. $(E_1 - E^\circ) \to -\infty$. Then, we selected E_2 in such a way that $(E_2 - E^\circ) \to +\infty$. Finally, we selected $E_3 = E_1$. Theoretical curves were obtained from the following equations:

(22) Rodriguez-Monge, L. M.; Muñoz, E.; Avila, J. L.; Camacho, L. *Anal. Chem.* **1988**, *60*, 2269.

(23) Baranski, A.; Fitak, S.; Galus, Z. *J. Electroanal. Chem. Interfacial Electrochem.* **1975**, *60*, 175.

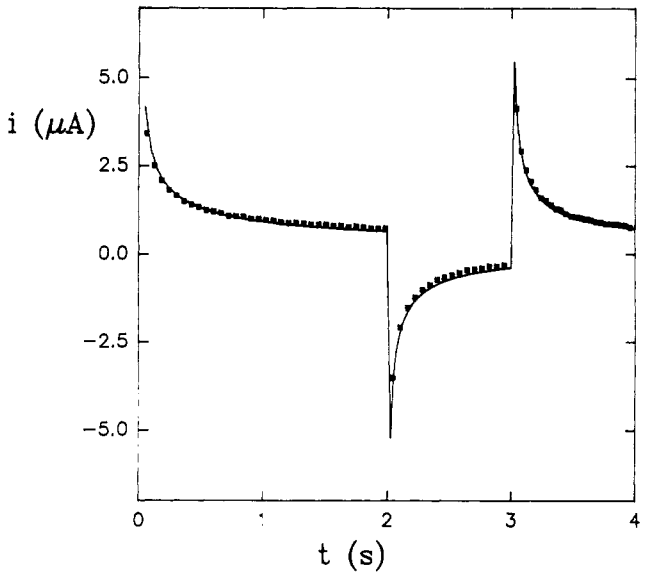

Figure 1. *i–t* curve for the reduction of 1 × 10^{-4} M Cd(II) in 0.1 M H_2SO_4. E_1 = −750 mV, t_1 = 2 s, E_2 = −500 mV, t_2 = 1 s, E_3 = −750 mV, t_3 = 1 s. Comparison between experimental (■) and theoretical (—) *i–t* curves.

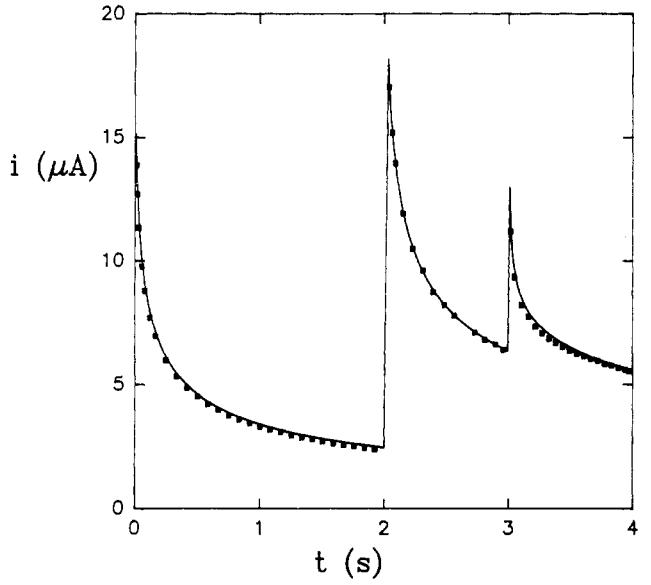

Figure 2. *i–t* curve for the reduction of 1 × 10^{-3} M Zn(II) in 1 M $NaNO_3$. E_1 = −1050 mV, t_1 = 2 s, E_2 = −1200 mV, t_2 = 1 s, E_3 = −1050 mV, t_3 = 1 s. Comparison between experimental (■) and theoretical (—) *i–t* curves.

$$i_1 = nFq_0\sqrt{\frac{D_A}{\pi t_1}}c_A^* \quad (32)$$

$$i_2 = nFq_0\sqrt{\frac{D_A}{\pi}}c_A^*\left(\left(\frac{1}{t_1+t_2}\right)^{1/2} - \left(\frac{1}{t_2}\right)^{1/2}\right) \quad (33)$$

$$i_3 = nFq_0\sqrt{\frac{D_A}{\pi}}c_A^*\left(\left(\frac{1}{t_1+t_2+t_3}\right)^{1/2} - \left(\frac{1}{t_2+t_3}\right)^{1/2} + \left(\frac{1}{t_3}\right)^{1/2}\right) \quad (34)$$

These equations were derived from eqs 3, 5, and 30, respectively, with $(E_1 - E^\circ) \to -\infty$, $(E_2 - E^\circ) \to -\infty$, and $k_s \to \infty$.

The solid line in the figure corresponds to the predictions of eqs 32–34 with D = 1.09 × 10^{-5} cm^2 s^{-1}, which was obtained by numerical fitting of the experimental results. As can be seen, there is a good correlation with the experimental results.

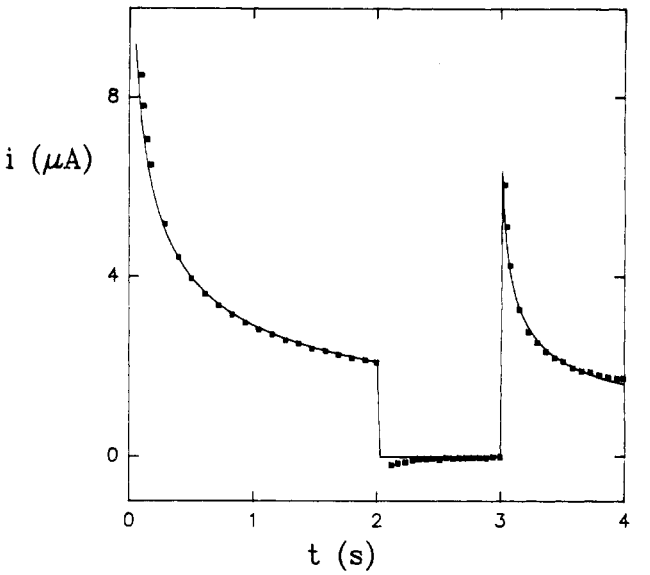

Figure 3. *i–t* curve for the reduction of 1 × 10^{-3} M Cr(III) in 1 M Na_2SO_4 + 0.1 M $HClO_4$. E_1 = −1200 mV, t_1 = 2 s, E_2 = −800 mV, t_2 = 1 s, E_3 = −1200 mV, t_3 = 1 s. Comparison between experimental (■) and theoretical (—) *i–t* curves.

The reduction of Zn(II) in 1 M $NaNO_3$ was chosen as the example of a quasi-reversible processes. In this case, D_B = 1.89 × 10^{-5} cm^2 s^{-1}, α = 0.233, and k_s = 4.59 × 10^{-3} cm s^{-1}.[13]

Figure 2 shows an example of *i–t* curves for Zn(II) obtained by using a potential pulse sequence such that diffusion conditions are never reached in order to show the quasi-reversibility of the process at potentials close to the normal reduction potential.

As can be seen, there is good fit between the experimental and theoretical data in all cases. The numerical fitting of the experimental results yielded E° = −1011 mV and D_A = 8.5 × 10^{-6} cm^2 s^{-1}.

We chose the reduction of Cr(III) in 1 M Na_2SO_4 + 0.01 M $HClO_4$ as the example of a completely irreversible processes ($D_A = D_B$). Figure 3 shows *i–t* curves for Cr(III) obtained by using the following pulse sequence: $E_1 = E_3$ and corresponded to a potential of the diffusion plateau of the process, whereas E_2 corresponded to a potential where neither the reduction nor the oxidation process takes place.

As in the previous cases, the solid line corresponds to the theoretical prediction with α = 0.57[24] and the values k_s = 1.75 × 10^{-5} cm s^{-1} and E° = −925 mV. Compared to the curves obtained under the same conditions for a reversible process (Figure 1), the curve in Figure 3 clearly shows the irreversible nature of the process involved. The numerical fitting of the experimental results yielded $D_A = D_B$ = 4.6 × 10^{-6} cm^2 s^{-1}. The experimental points at E_2 are not exactly zero at short times owing to the fact that the charging current was not eliminated.

From all these examples we can conclude that the predictions of the equations obtained for all triple-pulse sequences applied to the electrode are correct, irrespective of the nature of the electron transfer.

DISCUSSION AND SOME POTENTIAL APPLICATIONS OF THE SOLUTIONS

A triple pulse can be superimposed to a linear variation of the potential. Thus, we shall put forward some triple-pulse sequences in order to show some applications of eq 30.

(24) Andreu, R.; Sánchez, F.; González-Arjona, D.; Rueda, M. *J. Electroanal. Chem.* **1986**, *210*, 111.

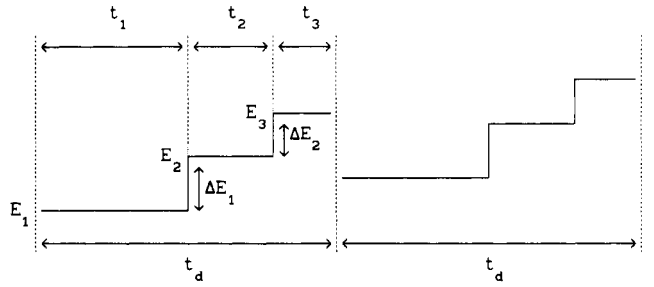

Figure 4. Potential–time waveform corresponding to the DDP technique.

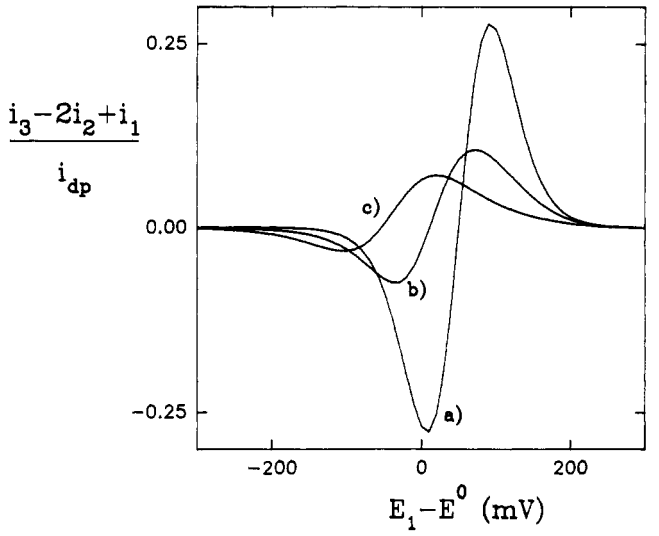

Figure 5. Plot of $(i_1 - 2i_2 + i_3)/i_{dp}$ vs $(E_1 - E^\circ)$ for $z = {}^2/_3$, $D_A = D_B = 10^{-5}$ cm^2 s^{-1}, $\Delta E_1 = \Delta E_2 = -50$ mV, $n = 1$, $\alpha = 0.5$, $t_1 = 5$ s, $t_2 = 0.50$ s, $t_3 = 0.033$ s, and k_s (cm^{-1} s) = (a) 1, (b) 3×10^{-3}, and (c) 10^{-4}.

First, we shall assume that the relation between the potentials E_1 and E_2 is the same as in the DP technique; i.e. E_1 remains constant over the time t_1, after which a new potential (E_2) is applied for a time t_2, $\Delta E_1 = E_2 - E_1$ being constant. Finally, a potential E_3 is applied over time t_3, $\Delta E_2 = E_3 - E_2$ also being constant. E_1, E_2, and E_3 are superimposed to a linear ramp of potentials and $t_d = t_1 + t_2 + t_3$. An example in which ΔE_1 and ΔE_2 are of the same sign is shown in Figure 4.

Obviously, $\Delta i_1 = i_2 - i_1$ corresponds to the DP (if $t_2 \ll t_1$) or DNP signal. If we call $\Delta i_2 = i_3 - i_2$ (where ΔE_1 and ΔE_2 are of opposite sign), the plot of Δi_1 and Δi_2 vs E_1 will have a form similar to that of the plot obtained in the DNP technique in its alternating pulse mode,[7] although the mathematical solutions of these techniques are not identical. As suggested by Birke,[8] a similar plot can be constructed in DP by just obtaining recordings with positive and negative pulses.

According to the previous relations, we define a new technique which will be called double differential pulse (DDP) from the relation $\Delta i_2 - \Delta i_1 = i_3 - 2i_2 + i_1$. The potential–time waveform is shown in Figure 4.

Figure 5 shows the plots of $(i_1 - 2i_2 + i_3)/i_{dp}$ (see Notation) vs $E_1 - E^\circ$ at $t_1 = 5$ s, $t_2 = 0.05$ s, $t_3 = 0.033$ s, and $\alpha = 0.5$ for different k_s values and $\Delta E_1 = \Delta E_2 = -50$ mV.

As can be seen, the shape of the curves is similar to the second derivative of the signal of the first pulse, although the properties of the DDP function are much more complex than those of a simple second derivative.

A second possibility involves assuming that E_1 and E_2 correspond to the pulse sequence used in the RP technique; i.e. E_1 is always constant and corresponds to a potential at which the reduction process is controlled by diffusion, whereas

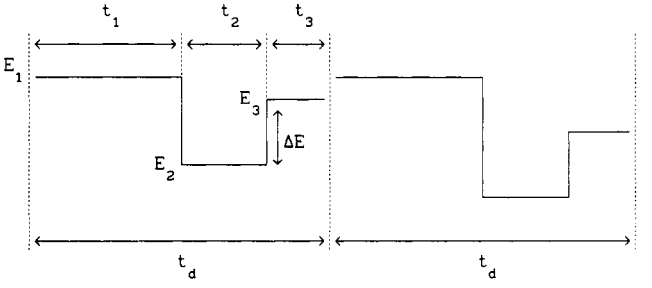

Figure 6. Potential–time waveform corresponding to the RDNP technique.

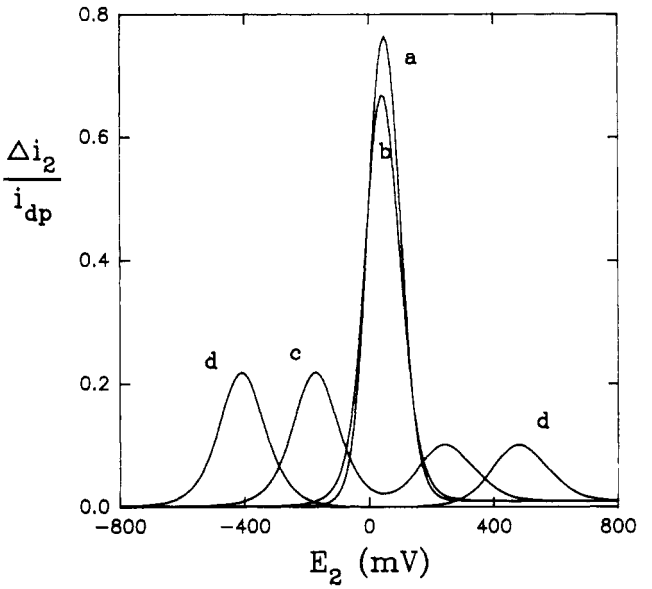

Figure 7. Plot of $\Delta i_2/i_{dp}$ vs E_2 with $\Delta E = -100$ mV, $E^\circ = 0$, $z = 0$, $D_A = D_B = 1 \times 10^{-5}$ cm^2 s^{-1}, $E_1 = -800$ mV, $t_1 = 1$ s, $t_2 = 0.3$ s, $t_3 = 0.03$ s, k_s (cm s^{-1}) = (a) 1, (b) 10^{-2}, (c) 10^{-4}, and (d) 10^{-6}.

E_2 shifts to anodic potentials. The signal used in the RP technique is given by $i_2 = i_{RP}$. If, under these circumstances, we choose a potential E_3 (see Figure 6) such that $\Delta E = E_3 - E_2$ is constant and plot $\Delta i_2 = i_3 - i_2$ as a function of E_2, we obtain curves that combine the properties of the RP techniques in relation to process resolution and of DP techniques in relation to charging current elimination and the Gaussian shape of the curves.

As noted in the Introduction, this technique was designated as RDNP in the literature[17] and so far had not been theoretically treated. Figure 7 shows some $\Delta i_2/i_{dp}$ vs E_2 plots obtained at $\alpha = 0.5$, $\Delta E = -100$ mV, $E_1 = -800$ mV, and different k_s values.

The curves in this figure are similar to the derivative of i_{RP} vs E_2, although the properties of Δi_2 are much more complex than those of a first derivative.

For comparison of these curves with the RP signal, Figure 8 shows an i_{RP}/i_{dc} (see Notation) vs E_2 plot obtained under the same conditions as Figure 7.

As can be seen in both figures, at small enough k_s values, the process splits into two: a more cathodic wave or peak, due to the reduction of the reactant, and a more anodic wave or peak, due to the oxidation of the reduced molecules. Figure 7 testifies to the enormous potential of this technique for kinetic purposes.

The options described above are based on modifications of DP and RP techniques. However, one can also use various pulse sequences for very different purposes. Thus, one can use a potential $E_1 = E_3$ that is modified linearly in consecutive mercury drops and a constant potential E_2 for all drops (see Figure 9). The value of E_2 is chosen in such a way that the

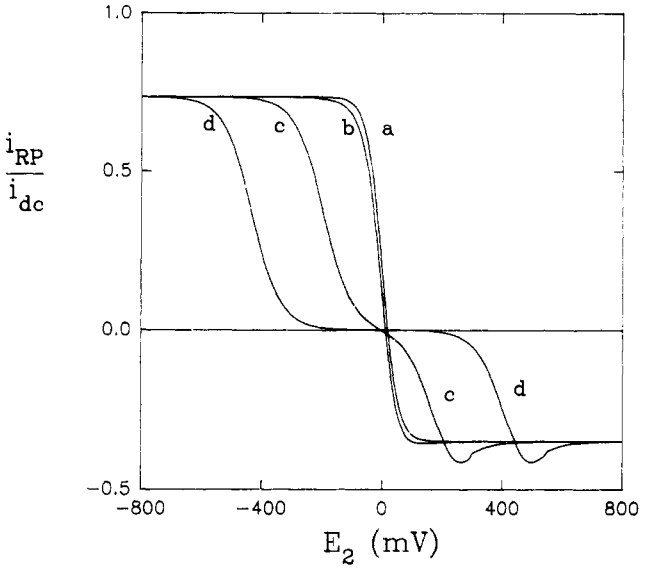

Figure 8. Plot of i_{RP}/i_{dc} vs E_2 with $E^\circ = 0$, $D_A = D_B = 1 \times 10^{-5}$ cm^2 s^{-1}, $t_1 = 1$ s, and $t_2 = 0.3$ s, $E_1 = -800$ mV, k_s (cm s^{-1}) = (a) 1, (b) 10^{-2}, (c) 10^{-4}, and (d) 10^{-6}.

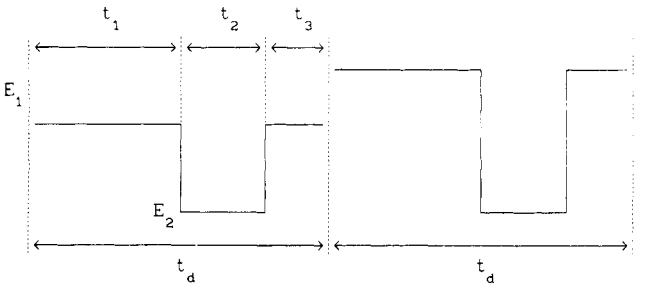

Figure 9. Potential–time waveform corresponding to the SWP technique.

reduction process does not take place.

If the oxidation process also does not take place at the potential E_2, then i_2 will be virtually nil, except in relation to the charging current. In this case, the behavior will be typical of an irreversible process.

On the other hand, if the oxidation takes place at potential E_2, then i_2 will be non-zero and the process will be reversible or quasi-reversible. Therefore, if the solutions contains two species with very close discharge potentials and a potential E_2 is chosen (such that only one of the spcies is oxidized but neither is reduced), then the current i_2 will be that corresponding to the species with a reversible or quasi-reversible behavior at E_2.

We shall use now a current linear combination $i_3 + i_2 - 2i_1$ in a pulse sequence such as that in Figure 9. This technique will be called square well pulse (SWP). If the electron transfer is completely reversible, then, for $t_1 \gg t_2 + t_3$ and from eqs 3, 5, and 30

$$F(i) = \frac{i_3 + i_2 - 2i_1}{i_{dp}} = \frac{1}{(1 + \gamma K_1)}\left(1 - \left(\frac{t_3}{t_2 + t_3}\right)^{1/2} - \left(\frac{t_3}{t_2}\right)^{1/2}\right) \quad (35)$$

$F(i) = 0$ if $t_3/t_2 = 0.283$. This function will be non-zero for an irreversible electron transfer. Therefore, with this function one can completely mask the signal corresponding to a reversible process.

Parts I and II of Figure 10 show the plots of $F(i)$ and i_2/i_{dc}, respectively, vs E_1 for different k_s values at $E^\circ = 0$ mV and $E_2 = 200$ mV in a pulse sequence such as that in Figure 9.

As can be seen, for a completely irreversible process (curves d) $i_2 = 0$ and $F(i) \neq 0$, whereas for a completely reversible process (curves a) $F(i) = 0$ and $i_2 \neq 0$. For intermediate k_s values, neither function is zero.

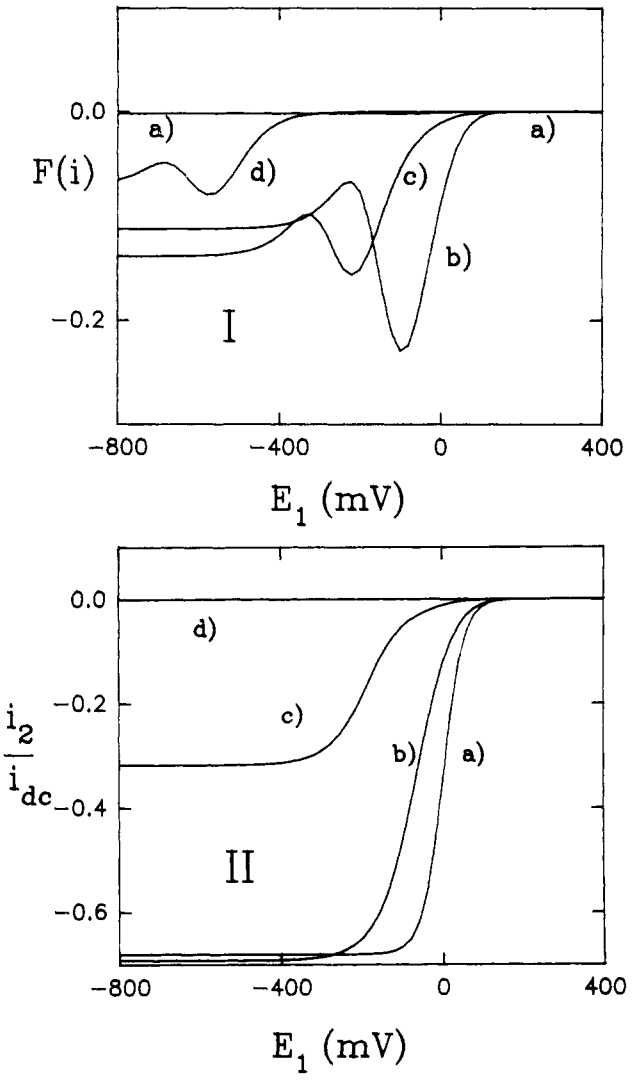

Figure 10. Plots of $F(i)$ (part I) and i_2/i_{dc} (part II) vs E_1 with $\alpha = 0.5$, $E_1 = E_3$, $E_2 = 200$ mV, $D_A = D_B = 1 \times 10^{-5}$ cm^2 s^{-1}, $t_1 = 1$ s, $t_2 = 0.05$ s, $t_3 = 0.14\,15$ s, k_3 (cm s^{-1}) = (a) 10^3, (b) 10^{-3}, (c) 10^{-4}, and (d) 10^{-7}.

Application of these sequences opens up vast possibilities from the analytical and kinetic points of view. In fact, two species with very close discharge potentials but different reduction mechanisms (reversible and irreversible) can be analyzed separately without interferences.

We can conclude that the solution of the faradaic response of a slow electron transfer to a triple pulse of potentials allows one to develop new voltammetric and polarographic techniques such as those of double differential pulse (DDP) and square well pulse (SWP). Likewise, it allows one to obtain the solution for the reverse differential normal pulse (RDNP) technique previously reported in the literature.

The analytical and kinetic features and performances of these techniques will be discussed in future papers.

ACKNOWLEDGMENT

The authors wish to express their gratitude to the DREUCA de la Región de Murcia, to the Junta de Andalucía, and to the DGICyT for financial help granted through Projects PB88-0283 and PB90-0307.

NOTATION

$K_i = \exp\left(\frac{nF}{RT}(E_1 - E^\circ)\right)$ $\gamma = \sqrt{D_A/D_B}$

$q(t) = q_0 t^z$ (time-dependent electrode area; $z = 0$ for a SMDE and $z = {}^2/_3$ for a DME)

k_f, k_b (heterogeneous rate constants for the forward and reverse charge-transfer reactions)

k_s (apparent heterogeneous rate constant for the charge transfe r at E°)

α (transfer coefficient)

$$\chi = \sqrt{\frac{4(t_1 + t_2 + \tau 3)}{(2z+1)D_A}} k_s \frac{1+\gamma K_1}{K_1^{\alpha}}$$

$$\chi_2 = \sqrt{\frac{4(t_1 + \tau 2)}{(2z+1)D_A}} k_s \frac{1+\gamma K_1}{K_1^{\alpha}}$$

$$s1_i = \sqrt{\frac{(2z+1)}{4tD_i}} x$$

$$s2_i = \frac{x}{2\sqrt{D_i(t - t_i)}}$$

$$\beta = (t_2 + \tau 3)/(t_1 + t_2 + \tau 3)$$

$$\beta_2 = (\tau 2)/(t_1 + \tau 2)$$

$$y = \sqrt{\frac{4(t_2 + \tau 3)}{D_A}} k_s \frac{1+\gamma K_2}{K_2^{\alpha}}$$

$$y_2 = \sqrt{\frac{4\tau 2}{D_A}} k_s \frac{1+\gamma K_2}{K_2^{\alpha}}$$

$F_z(x) =$

$$\sum_{j=0}^{} \frac{(-1)^j x^{(j+1)}}{\prod_{i=0}^{j} p_i(z)}$$ (Koutecky function of argument z, x)

$G_z(\beta,x)$ (Gálvez function of argument z, β, x)

$$G_{2/3}(u,x) = \sum_{j=0}^{} \frac{(-1)^j x^{(j+1)}}{\prod_{i=0}^{j} p_i^{(0)}} \times \left(1 - \frac{ju}{3(j+2)} - \frac{j(2j+9)u^2}{18(j+2)(j+4)} - \frac{5j(j+5)u^3}{81(j+2)(j+6)} - \ldots\right)$$

$$G_0(u,x) = G_z(0,x) = F_0(x) = \sqrt{\pi}\frac{x}{2}\exp\left(\frac{x^2}{4}\right)\operatorname{erfc}(x/2)$$

$$i_{dc} = nFq_0(t_1 + t_2)^z \sqrt{\frac{D_A}{\pi t_2}} c_A^*$$

$$i_{dp} = nFq_0(t_1 + t_2 + t_3)^z \sqrt{\frac{D_A}{\pi t_3}} c_A^*$$

APPENDIX

For a DME ($z = {}^2/_3$), eqs 19–29 and 21–26 for $\sigma_{j,k,m}(s3_A)$ if $t_3 \ll t$ yield

For $j = 2n$, $n = 0, 1, 2, \ldots$ (where the subscript $k = 0$ has been suppressed by simplicity)

$$\sigma_{2n,0}(s3_A) = 0 \quad \text{(A-1)}$$

At $m > 0$ the functions $\sigma_{2n,m}(s3_A)$ coincide with the $\phi_{0,n,m}$ functions derived in ref 25 if ω^* is replaced with $c_A^* Z_2$.

For $j = 2n + 1$, $n = 0, 1, 2, \ldots$

$$\sigma_{1,m}(s3_A) = X_m \psi_{m+1}(s3_A) \quad \text{(A-2)}$$

$$\sigma_{3,m}(s3_A) = -X_m\left[\frac{m+1}{3}\psi_{m-1}(s3_A) - \frac{4m+7}{6}\psi_{m+1}(s3_A) + \frac{m^2+5m+7}{3(m+3)}\psi_{m+3}(s3_A)\right] \quad \text{(A-3)}$$

$$\sigma_{5,m}(s3_A) = X_m\left[\frac{(m+1)(m-1)}{18}\psi_{m-3}(s3_A) - \frac{(m+1)(12m+19)}{54}\psi_{m-1}(s3_A) + \frac{8m^2+40m+49}{24}\psi_{m+1}(s3_A) - \frac{4m^3+41m^2+133m+147}{18(m+3)}\psi_{m+3}(s3_A) + \frac{3m^4+52m^3+324m^2+851m+822}{54(m+3)(m+5)}\psi_{m+5}(s3_A)\right] \quad \text{(A-4)}$$

$$\sigma_{7,m}(s3_A) = -X_m\left[\frac{(m+1)(m-1)(m-3)}{162}\psi_{m-5}(s3_A) - \frac{(m+1)(m-1)(12m+17)}{324}\psi_{m-3}(s3_A) + \frac{(m+1)(60m^2+284m+325)}{648}\psi_{m-1}(s3_A) - \frac{160m^3+1592m^2+4996m+5145}{1296}\psi_{m+1}(s3_A) + \frac{60m^4+1024m^3+6213m^2+15941m+15435}{648(m+3)}\psi_{m+3}(s3_A) - \frac{12m^5+313m^4+3116m^3+14744m^2+33313m+30870}{324(m+3)(m+5)}\psi_{m+5}(s3_A) + \frac{m^6+37m^5+548m^4+4131m^3+16668m^2+34433m+30870}{162(m+3)(m+5)(m+7)}\psi_{m+7}(s3_A)\right] \quad \text{(A-5)}$$

For a stationary planar electrode ($z = 0$), we have

For $j = 2n$, $n = 0, 1, 2, \ldots$

$$\sigma_{2n,m}(s3_A) = 0 \quad \text{unless } n = 0,\ m \geq 1 \quad \text{(A-6)}$$

$$\sigma_{0,m}(s3_A) = \frac{(-1)^m c_A^* Z_2}{\prod_{i=1}^{m} p_i(0)}\psi_m(s3_A) \quad \text{(A-7)}$$

For $j = 2n + 1$, $n = 0, 1, 2, \ldots$

$$\sigma_{1,m}(s3_A) = X_m \psi_{m+1}(s3_A) \quad \text{(A-8)}$$

$$\sigma_{3,m}(s3_A) = X_m\left[\frac{1}{2}\psi_{m+1}(s3_A) - \frac{1}{m+3}\psi_{m+3}(s3_A)\right] \quad \text{(A-9)}$$

$$\sigma_{5,m}(s3_A) = X_m\left[\frac{3}{8}\psi_{m+1}(s3_A) - \frac{3}{2(m+3)}\psi_{m+3}(s3_A) + \frac{3}{(m+3)(m+5)}\psi_{m+5}(s3_A)\right] \quad \text{(A-10)}$$

$$\sigma_{7,m}(s3_A) = X_m\left[\frac{5}{16}\psi_{m+1}(s3_A) - \frac{15}{8(m+3)}\psi_{m+3}(s3_A) + \frac{15}{2(m+3)(m+5)}\psi_{m+5}(s3_A) - \frac{15}{(m+3)(m+5)(m+7)}\psi_{m+7}(s3_A)\right] \quad \text{(A-11)}$$

with

$$X_m = \frac{(-1)^m c_A^* S}{\prod_{i=1}^{m+1} p_i(0)} \quad \text{(A-12)}$$

where $\psi_i(s3_A)$ are the Koutecky functions[21] and S is given by eq 27 and

$$p_i(z) = \frac{\Gamma\left(1 + \frac{i}{4z+2}\right)}{\Gamma\left(\frac{1}{2} + \frac{i}{4z+2}\right)} \quad \text{(A-13)}$$

Γ being the Euler gamma function.

The functions $\sigma_{0,k,m}(s3_A)$ are given by eqs A-7–A-12 for any z value, if S in X_m is replaced with D. Moreover, the $\sigma_{j,k,m}(s3_A)$ functions with j and $k \geq 1$ are zero.

Asymptotic Solution. For large ω values it is more appropriate to obtain an asymptotic solution by replacing y with $1/y$ and ω with $1/\omega$ in eqs 17 and 18. Thus, the functions $\sigma_{2n,m}(s3_A)$ ($n = 0, 1, 2, \ldots$) for $z = {}^2/_3$ coincide with the $\phi_{0,n,m}$ asymptotic functions derived in ref 25 if ω^* is replaced with $c_A^* Z_2$. The $\sigma_{2n+1,m}(s3_A)$ ($n = 0, 1, 2, \ldots$) functions for $m \geq 1$ are identical with the above eqs A-1–A-5 if m is replaced with $-m$ and X_m with W_m.

$$\left.\begin{aligned} W_m &= (-1)^{m+1} c_A^* S \prod_{i=0}^{m-2} p_{-i}(0) \qquad m > 1 \\ W_1 &= c_A^* S \end{aligned}\right\} \quad \text{(A-14)}$$

$$\text{For } m = 0 \qquad \sigma_{2n+1,0}(s3_A) = 0 \quad \text{(A-15)}$$

For a stationary planar electrode ($z = 0$), the $\sigma_{2n,m}(s3_A)$ ($n = 0, 1, 2, \ldots$) functions are

$$\sigma_{0,m}(s3_A) = c_A^* Z_2 w_m P_{-m+1}(0)\psi_{-m} \qquad m \geq 0 \quad \text{(A-16)}$$

$$\sigma_{2n,m}(s3_A) = 0 \qquad n > 0 \quad \text{(A-17)}$$

The $\sigma_{2n+1,m}(s3_A)$ functions for $m \geq 1$ can be derived from eqs A-7–A-12 by performing the same substitutions as for the expanding planar electrode models, and for $m = 0$

$$\sigma_{2n+1,0}(s3_A) = 0 \quad \text{(A-18)}$$

Moreover, the σ and ρ functions are such that, in all cases

$$\gamma\sigma_{j,m}(s3_B) = \varphi_{j,m}(s3_B) \quad \text{(A-19)}$$

Finally, in order to determine the values of the σ functions at $s3_A = 0$, we shall take into account that the uncertainties of the form $0\cdot\infty$ in the product $P_{-k}\psi_{-2k}$ can be readily solved by using the properties of the Koutecky functions $\psi_j(s_j)$.[21,26]

We also used the relation

$$\lim_{k\to m}(m-k) = \pm p_{-1}/p_1 \quad \text{(A-20)}$$

in which the upper sign relates to direct treatment and the lower sign to the asymptotic one.

By substituting equations corresponding to the σ and ρ functions into eqs 13, 17, and 18, we arrive at eq 30 for $i_3(t)$. In this equation, the Koutecky function $F_z(x)$ is given in ref 11 and as approximate form in ref 27. The Gálvez function $G_z(\beta,x)$ is given in ref 11 and as an approximate function in ref 28 (see Notation).

Finally, the series $H_z(n,x)$ is given by

$$H_0(n,x) = \sum_{m=0}^{\infty}\frac{(-1)^m x^{m+1}}{\prod_{i=0}^{m} p_i(0)}\left[1 + \frac{m}{2(m+2)}n + \frac{3m}{8(m+4)}n^2 + \frac{5m}{16(m+6)}n^3 + \ldots\right] \quad \text{(A-21)}$$

and for $x \gg 1$

$$H_0(n,x) = \left(1 - \frac{1}{2}n - \frac{1}{8}n^2 - \frac{1}{16}n^3\right) + P_1 n x^{-1} - \left(2 + 3n - \frac{9}{4}n^2 - \frac{5}{8}n^3\right)x^{-2} - 6P_1 n^2 x^{-3} + \left(12 + 10n + \frac{45}{2}n^2 - \frac{75}{4}n^3 + \ldots\right)x^{-4} \quad \text{(A-22)}$$

$$H_{2/3}(n,x) = \sum_{m=0}^{\infty}\frac{(-1)^m x^{m+1}}{\prod_{i=0}^{m} p_i(0)}\left[1 + \frac{m}{6(m+2)}n + \frac{m(6m+7)}{72(m+2)(m+4)}n^2 + \frac{7m(13m-34)}{1296(m+2)(m+6)}n^3 + \ldots\right] \quad \text{(A-23)}$$

and for $x \gg 1$

$$H_{2/3}(n,x) = \left(1 - \frac{1}{6}n + \frac{13}{216}n^2 + \frac{329}{6480}n^3 + \ldots\right) + \frac{1}{3}P_1 n\left(1 - \frac{5}{6}n - \frac{35}{72}n^2 - \ldots\right)x^{-1} - \left(2 + n - \frac{9}{4}n^2 - \frac{511}{648}n^3 - \ldots\right)x^{-2} - \frac{34}{9}P_1 n^2 x^{-3} + \left(12 + \frac{10}{3}n + \frac{205}{18}n^2 - \frac{385}{36}n^3 + \ldots\right)x^{-4} \quad \text{(A-24)}$$

RECEIVED for review March 19, 1992. Accepted October 15, 1992.

(25) Gálvez, J.; Serna, A. *J. Electroanal. Chem. Interfacial Electrochem.* **1976**, *69*, 145.
(26) Brinkman, A. A. A. M.; Los, J. M. *J. Electroanal. Chem.* **1964**, *7*, 171.
(27) Oldham, K. B.; Parry, E. P. *Anal. Chem.* **1968**, *40*, 65.
(28) Camacho, L.; Avila, J. L.; Heras, A. M.; García-Blanco, F. *J. Electroanal. Chem. Interfacial Electrochem.* **1985**, *182*, 173.